Open Access Full Text Article

ORIGINAL RESEARCH

RIPL peptide-conjugated nanostructured lipid carriers for enhanced intracellular drug delivery to hepsin-expressing cancer cells

Sang Gon Lee[1],*
Chang Hyun Kim[1],*
Si Woo Sung[1]
Eun Seok Lee[1]
Min Su Goh[1]
Ho Yub Yoon[1]
Myung Joo Kang[2]
Sangkil Lee[3]
Young Wook Choi[1]

[1]College of Pharmacy, Chung-Ang University, Seoul, Republic of Korea; [2]College of Pharmacy, Dankook University, Chungnam, Republic of Korea; [3]College of Pharmacy, Keimyung University, Daegu, Republic of Korea

*These authors contributed equally to this work

Correspondence: Young Wook Choi
College of Pharmacy, Chung-Ang University, 221 Heuksuk-dong, Dongjak-gu, Seoul 156-756, Republic of Korea
Tel +82 2 820 5609
Fax +82 2 826 3781
Email ywchoi@cau.ac.kr

Background: To facilitate selective and enhanced drug delivery to hepsin (Hpn)-expressing cancer cells, RIPL peptide (IPLVVPLRRRRRRRRC, 16-mer)-conjugated nanostructured lipid carriers (RIPL-NLCs) were developed.

Methods: NLCs were prepared using a solvent emulsification-evaporation method and the RIPL peptide was conjugated to the maleimide-derivatized NLCs via the thiol-maleimide reaction. Employing a fluorescent probe (DiI), in vitro target-selective intracellular uptake behaviors were observed using fluorescence microscopy and flow cytometry. Separately, docetaxel (DTX) was encapsulated by pre-loading technique, then cytotoxicity and drug release were evaluated. In vivo antitumor efficacy was investigated in BALB/c nude mice with SKOV3 cell tumors after intratumoral injections of different DTX formulations at a dose equivalent to 10 mg/kg DTX.

Results: RIPL-NLCs showed positively charged nanodispersion, whereas NLCs were negatively charged. DTX was successfully encapsulated with an encapsulation efficiency and drug loading capacity of 95–98% and 44-46 µg/mg, respectively. DTX release was diffusion-controlled, revealing the best fit to the Higuchi equation. Cellular uptake of DiI-loaded RIPL-NLCs was 8.3- and 6.2-fold higher than that of DiI-loaded NLCs, in Hpn(+) SKOV3 and LNCaP cells, respectively. The translocation of RIPL-NLCs into SKOV3 cells was time-dependent with internalization within 1 h and distribution throughout the cytoplasm after 2 h. DTX-loaded RIPL-NLCs (DTX-RIPL-NLCs) revealed dose-dependent in vitro cytotoxicity, while drug-free formulations were non-cytotoxic. In SKOV3-bearing xenograft mouse model, DTX-RIPL-NLCs significantly inhibited tumor growth: the inhibition ratios of the DTX solution-treated and DTX-RIPL-NLC-treated groups were 61.4% and 91.2%, respectively, compared to those of the saline-treated group (control).

Conclusion: RIPL-NLCs are good candidates for Hpn-selective drug targeting with a high loading capacity of hydrophobic drug molecules.

Keywords: nanostructured lipid carriers, RIPL peptide, intracellular delivery, docetaxel, antitumor efficacy, targeting

Introduction

To date, because of their main limitations, including low solubility and non-specific distribution throughout the body, conventional cancer chemotherapeutics have exhibited poor antitumor activity and serious side effects. To overcome these obstacles, various delivery systems, including lipid-based nanocarriers, have been widely investigated in oncology to encapsulate poorly soluble drugs, to enhance their physicochemical stability, to increase their blood circulation time, and to offer selectivity to target cells.[1,2] Lipid-based nanocarrier systems such as solid lipid nanoparticles and nanostructured lipid carriers (NLCs) have attracted attention and are extensively

applied in chemotherapeutic drug delivery as an alternative to traditional colloidal carriers such as liposomes and micelles. NLCs are composed of a blend of solid lipid and liquid oil and carry several advantages over liposomal carrier systems, such as a high loading capacity for hydrophobic drugs,[3] improved physical stability of the nanoparticles,[4] controlled drug release properties,[5] and increased chemical stability of the incorporated drugs.[6] However, because of their non-specificity, NLCs still need to be further functionalized for targeted drug delivery.

Active targeting with surface-modified nanocarriers has been highlighted as a promising mechanism for the selective and enhanced delivery of chemotherapeutics. By employing targeting moieties that can recognize target sites or cells, the nanocarriers bind to the specific molecules overexpressed at the diseased sites by ligand–receptor or antigen–antibody interactions.[7–9] Hepsin (Hpn), a member of the Hpn/TMPRSS/enteropeptidase subfamily of the type II transmembrane serine proteases, has recently been addressed as a biomarker to detect early prostate cancer.[10] This extracellular protease is upregulated in prostate cancer cells but is either absent or expressed at very low levels in normal prostate and/or benign prostatic hypertrophy cells.[11] Based on this difference, IPLVVPL peptide has been introduced as a cell-targeting peptide (CTP) possessing both a high affinity and a high selectivity for Hpn.[12]

However, because CTP alone was previously insufficient to enhance the internalization of cargos, a combination of cell-penetrating peptides and CTPs has been widely introduced for the surface modification of nanocarriers.[13,14] These peptides are linked to the surface of nanocarriers via specific ligand modifications of either the dual-ligand or linear-ligand type.[15,16] Recently, we successfully developed RIPL peptide (IPLVVPLRRRRRRRRC, 16-mer), a linear-type, chimeric, cell-penetrating homing peptide (CPHP), that can recognize a target (Hpn) and simultaneously enhance the intracellular delivery of cargo into the Hpn-expressing cancer cells.[11] RIPL peptide-modified liposomes exhibited excellent Hpn selectivity, and by loading an anticancer drug, docetaxel (DTX), resulted in significant tumor growth inhibition (TGI) and prolonged survival time in a xenograft mouse model.[16] Nevertheless, the DTX loading capacity of the liposomes was very limited, revealing an encapsulation efficiency (EE) of 32%–36%, due to the hydrophobicity of the drug molecule. Thus, improvement in DTX loading was necessary for further drug development.

In the present work, NLCs were employed as an alternative carrier and surface-modified with RIPL peptide to facilitate selective drug delivery. The physicochemical properties of the RIPL peptide-conjugated NLCs (RIPL-NLCs) were characterized in terms of their particle size, zeta potential (ZP), EE for DTX, and drug loading (DL). Transmission electron microscopy (TEM) and differential scanning calorimetry (DSC) were conducted, and drug release kinetics was observed. The cellular uptake behavior and cytotoxicity of the RIPL-NLCs were evaluated by using Hpn-expressing (Hpn(+); SKOV3 and LNCaP) and Hpn-non-expressing (Hpn(−); DU145 and PC-3) cells. Finally, in vivo antitumor efficacy was assessed after intratumoral injections of the formulations into xenograft mouse models.

Materials and methods
Materials
DTX (purity >99%) was kindly provided by Chong Kun Dang Pharm. Co. (Yongin, Korea). Precirol® ATO 5 (glyceryl distearate) and Labrafil® M 1944 CS (oleoyl macrogol-6 glycerides) were obtained as a gift from Gattefosse (Saint-priest, France). Tween® 20 (polysorbate 20), Tween® 80 (polysorbate 80), polyvinylalcohol (PVA), dichloromethane, phosphate-buffered saline (PBS) tablets, 5,50-dithio-bis(2-nitrobenzoicacid) (DTNB), and 1,1′-dioctadecyl-3,3,3′,3′-tetramethylindocarbocyanine perchlorate (DiI) were purchased from Sigma-Aldrich Co. (St Louis, MO, USA). Distearoyl phosphatidylethanolamine-polyethylene glycol2000-maleimide (DSPE-PEG$_{2000}$-Mal; DP2M), was purchased from Avanti Polar Lipids (Alabaster, AL, USA). RIPL peptide was synthesized and purchased from Peptron Co. (Daejeon, Korea).

For cell experiments, cell lines were purchased from the Korean Cell Line Bank (Seoul, Korea). PBS solution (pH 7.4, 10×) and cell culture materials including Roswell Park Memorial Institute (RPMI) medium 1640, Dulbecco's Modified Eagle's Medium, fetal bovine serum (FBS), penicillin-streptomycin, and trypsin-ethylenediaminetetraacetic acid (EDTA, 0.25%) were obtained from Thermo Fisher Scientific (Waltham, MA, USA). NUNC CC2 glass slide, chambered cover glass, and 16% formaldehyde solution were purchased from Thermo Scientific Nunc (Rochester, NY, USA). VECTASHIELD mounting medium with 4′,6-diamidino-2-phenylindole (DAPI) was purchased from Vector Laboratories, Inc. (H-1200, Burlingame, CA, USA). EZ-cytox cell viability assay solution WST-1® was purchased from Daeil Lab Service (Seoul, Korea). For animal experiments, BD Matrigel™ Basement Membrane Matrix was purchased from BD Biosciences (San Jose, CA, USA). Female BALB/c athymic mice (5–6 weeks, 20±2 g) were purchased from HanLim Experimental Animal Laboratory (Gyeonggi-do, Korea). The animal experiment was approved by the Institutional Animal Care and Use Committee of Chung-Ang University in Seoul, Korea and was carried out according to the National Institute of Health guidelines. All

other chemicals and reagents purchased from commercial sources were of analytical or cell culture grade.

Synthesis and identification of RIPL peptide

RIPL peptide was synthesized by using a previously described 9-fluorenylmethyloxycarbonyl (Fmoc) solid phase peptide synthesis method.[12] In brief, amino acid units were coupled one by one from the C-terminal by using an automated peptide synthesizer (ASP48S, Peptron Co.). The amino acids used in the peptide synthesis were all protected by trityl, t-butyl, t-butyloxycarbonyl, and the like, whereby the N-terminal is protected by Fmoc, and the residues are all removed in acid. Synthesized RIPL peptide was purified by reverse phase high-performance liquid chromatography (HPLC) (Shimadzu, Kyoto, Japan). Preparative HPLC purification by gradient elution was performed. The molecular ion peak of the purified RIPL peptide was measured as 2,102 (calculated molecular weight [MW] 2,101.32) by liquid chromatography/mass spectrometry (LC/MS; Agilent HP1100 series, Palo Alto, CA, USA).

Preparation of DTX-loaded NLCs

DTX-loaded NLC (DTX-NLC) was prepared by using a solvent emulsification–evaporation method. DTX, Precirol®

ATO 5 (solid lipid), and Labrafil M 1944 CS (liquid oil) were dissolved in dichloromethane and then mixed with an aqueous emulsifier solution composed of PVA and Tween 20. The mixture was homogenized by using an Ultra-Turrax® T25 basic (IKA Labortechnik, Staufen, Germany) at 15,000 rpm for 2 min, and the emulsion was sonicated by using a bath type sonicator (Branson 2210R-DTH; Branson Ultrasonics Corporation, Danbury, CT, USA) for 60 min at 5°C. Next, the organic solvent of the emulsion was evaporated by stirring with a magnetic stirring bar at 400 rpm for 3 h. Drug-free NLC was also prepared by using the same procedure, except for the addition of DTX. Separately, to investigate the cellular uptake of NLC, DTX was replaced with DiI, a red hydrophobic fluorescent probe, following the same procedure as above. Prepared NLCs were stored at 4°C and used for the experiments within 2 weeks.

Preparation of DTX-loaded RIPL-NLCs

DTX-loaded RIPL-NLC (DTX-RIPL-NLC) was prepared by conjugating RIPL peptide to maleimide-derivatized DTX-NLC via a thiol-maleimide reaction, as previously reported.[12] The schematic illustration of RIPL-NLC preparation and the representative structure of a DTX-RIPL-NLC are depicted in Figure 1. The maleimide-derivatized DTX-NLC was prepared by using a solvent emulsification–evaporation
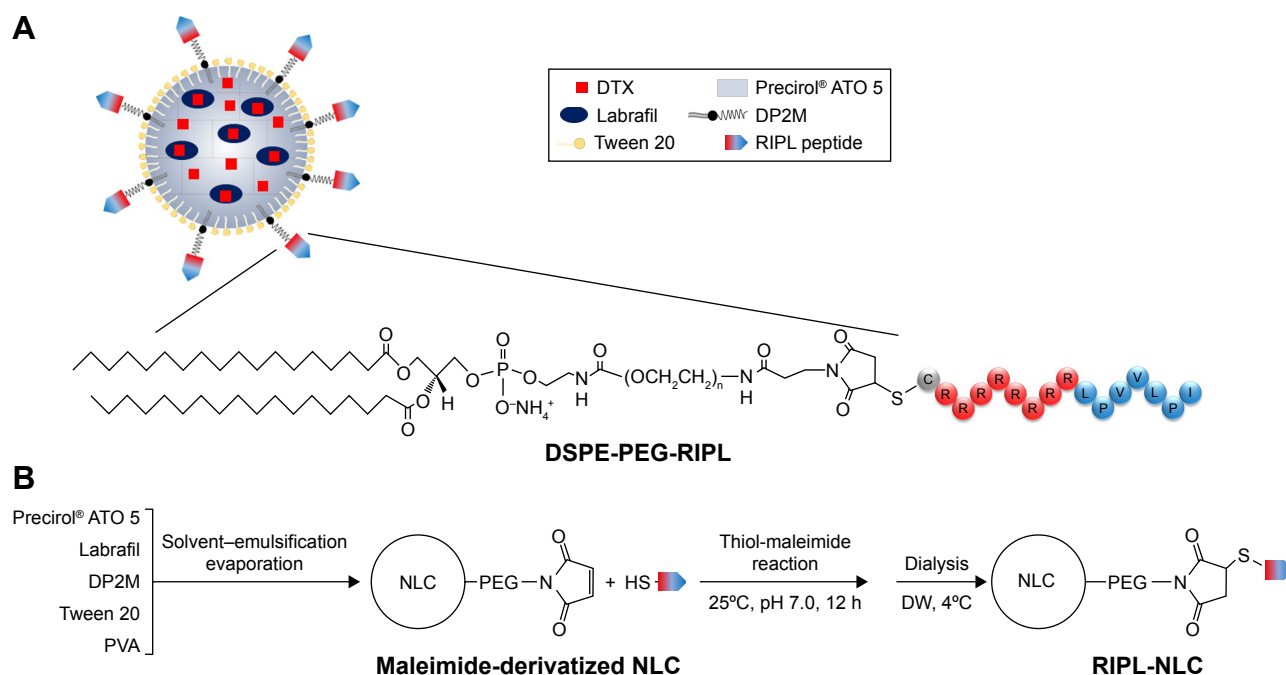

Figure 1 Schematic illustration of RIPL-NLC preparation.
Notes: (**A**) Representative structure of DTX-RIPL-NLC. (**B**) Schematic procedure for preparing RIPL-NLC.
Abbreviations: DP2M, distearoyl phosphatidylethanolamine-polyethylene glycol2000-maleimide; DTX, docetaxel; DTX-RIPL-NLC, docetaxel-loaded RIPL peptide-conjugated nanostructured lipid carrier; DW, distilled water; NLC, nanostructured lipid carrier; PVA, polyvinylalcohol; RIPL-NLC, RIPL peptide-conjugated nanostructured lipid carrier.

method, as described above. Briefly, DSPE-PEG$_{2000}$-Mal was dissolved in organic solvent with DTX, solid lipid, and liquid oil. Next, the lipid phase was mixed with the aqueous phase composed of PVA and Tween 20. The mixture was homogenized at 15,000 rpm for 2 min, then sonicated for 60 min at 5°C, and evaporated for 3 h by stirring. Subsequently, the RIPL peptide was added to the maleimide-derivatized DTX-NLC dispersion and allowed to react for 12 h at room temperature. DTX-RIPL-NLC was purified from unreacted RIPL peptide by dialysis against distilled water through a cellulose ester dialysis membrane (50 kDa MWCO) for 24 h at 4°C. Drug-free RIPL-NLC was also prepared by using the same procedure, except for the addition of DTX. Unreacted RIPL was assayed by HPLC analysis to estimate the degree of conjugation. Separately, to investigate the cellular uptake of RIPL-NLC, DTX was replaced with DiI following the same procedure as above. Prepared RIPL-NLCs were stored at 4°C and used for the experiments within 2 weeks.

Preparation of DTX solution as a reference

To mimic the marketed formulation of DTX, Taxotere® (Sanofi-aventis, Laval, QC, Canada), DTX solution (DTX-Sol) was prepared as a reference. DTX was dissolved in distilled water containing 25% (w/v) of Tween 80 and 9.75% (v/v) of ethanol at a concentration of 10 mg/mL. For in vitro cytotoxicity studies and in vivo intratumoral injections, DTX-Sol was diluted with culture media and saline at determined concentrations, respectively.

Particle size and ZP analysis

The various NLCs were diluted 1,000 times with distilled water and examined for particle size, size distribution, and ZP by dynamic light scattering (DLS), by using a Zetasizer Nano-ZS ZEN3600 (Malvern Instruments, Malvern, UK) which was equipped with a 50 mV laser at a scattering angle of 90°. Values were calculated from measurements performed in triplicate.

Calculation of fixed aqueous layer thickness (FALT)

The FALT of NLCs was calculated by using Gouy-Chapman theory.[18] According to the theory, ZP Ψ (L) as the electrostatic potential at the position of the slipping plane L (nm) is expressed as the following equation: $\ln \Psi(L) = \ln A - \kappa L$, where A is a constant and κ is the Debye–Hückel parameter, equal to $\sqrt{(C)}/0.3$, in which C is the molality of electrolytes. Using NaCl as the electrolyte at concentrations of 0, 0.01, 0.05, and 0.1 M, ZPs were measured and plotted against κ to calculate the slope L that indicates the position of the slipping plane or the thickness of the fixed aqueous layer in nanometer units.

Determination of EE and DL

The EE and DL of DTX in various NLC formulations were determined by ultrafiltration by using Amicon® Ultra-0.5 centrifugal filter devices (MWCO 100 kDa; EMD Millipore, Billerica, MA, USA). Briefly, 0.5 mL of each DTX-loaded lipid-based nanocarrier dispersion was placed in the upper chamber. Then, the ultrafilters were centrifuged (Smart R17; Hanil Science, Gyeonggi-do, Korea) for 20 min at 14,000× g. Free drug concentration was measured by HPLC. The following equations were used for the calculations:

$$EE\ (\%) = \frac{W_T - W_F}{W_T} \times 100$$

$$DL\ (\mu g/mg) = \frac{W_T - W_F}{W_L}$$

where W_T, W_F, and W_L represent the total amount of the DTX added, the amount of free DTX, and the total amount of the lipids, respectively.

HPLC assay of DTX and DiI

Quantitative determination of DTX was performed by using an HPLC system consisting of separating modules (Waters® e2695), a UV detector (Waters® e2489), and a data station (Empower® 3), which were purchased from Waters® Corporation (Milford, MA, USA). DTX was separated by using a C18 Column (Kromasil®, 5 μm, 4.6 × 250 mm) with acetonitrile and water (55:45, v/v) as a mobile phase and delivered at a flow rate of 1 mL/min at room temperature. DTX was detected at 230 nm, and the injection volume was 50 μL. Separately, the amount of DiI was also quantified by using the same HPLC system with the exception of the fluorescence detector (Waters® W2475). Chromatography was carried out on a C18 Column (Shiseido, Tokyo, Japan) with 0.05 M dimethyl sulfate and methanol (2:98, v/v) as a mobile phase. The excitation and emission wavelengths were set at 549 and 565 nm, respectively.

Conformational characterization of ligand conjugation

The number of external maleimide groups was calculated indirectly by determining the amount of unreacted cysteine in an Ellman's reaction as previously reported.[12,19] Briefly,

maleimide-derivatized NLCs were incubated with a three-fold molar amount of cysteine hydrochloride anhydrous, and a known amount of DTNB (1.0 mg/mL) was added to react with the unreacted cysteine, leading to the formation of a cysteine-TNB (5-thio-2-nitrobenzoic acid) adduct to cause the concomitant release of an equivalent of free TNB. The amount of liberated TNB was analyzed by using the HPLC system as above at the flow rate of 1.0 mL/min and ultraviolet (UV) detection at 420 nm. The mobile phase was composed of a mixture of methanol and 10 mM ammonium formate solution (5:95 v/v). Separately, the extent of RIPL peptide conjugation to maleimide-derivatized NLCs was calculated indirectly by determining the amount of unconjugated RIPL peptide by HPLC. Briefly, unpurified RIPL-NLC dispersion (0.5 mL) was ultra-centrifuged (20 min; 14,000× g) by using a centrifugal filter device (MWCO 100 kDa; Amicon® Ultra-0.5). Chromatographic separation of unreacted RIPL by gradient elution was performed on a C18 column (4.6 × 50 mm; 5 μm) and UV detection at 420 nm with a mobile phase of 0.1% trifluoroacetic acid in water (eluant A) and 0.1% trifluoroacetic acid in acetonitrile (eluant B). The eluant gradient increased from 3% to 50% B in 12 min at the flow rate of 1.0 mL/min, and the peptide peak was separated with a retention time of 6.2 min.

TEM

The morphology of DTX-NLC and DTX-RIPL-NLC was examined by using a TEM (JEM1010; JEOL, Tokyo, Japan) with an acceleration voltage of 80 kV. Prior to staining, samples were diluted 1,000-fold by using distilled water and placed onto a carbon film covered with a copper grid. Then, the samples were stained with 2% uranyl acetate. After washing with distilled water and drying at room temperature, the replica on the grid was prepared on a sample holder and then placed in the vacuum chamber of the TEM device.

DSC

The melting behavior of DTX, DTX-NLC, DTX-RIPL-NLC, and Precirol® ATO 5 was examined by using DSC (DSC-Q1000; TA Instruments, New Castle, DE, USA). All samples were dried before DSC measurement and the dried nanocarriers (2–3 mg) were put into aluminum pans. The samples were scanned as the temperature rose from 0°C to 200°C at a heating rate of 5°C/min.

Colloidal stability of NLCs

The physical stability of NLCs was monitored for 2 weeks by the changes in size and ZP on storage at 4°C. Separately, serum stability of DTX-loaded NLCs was observed as reported elsewhere.[20] Briefly, prepared NLC samples were incubated with distilled water (DW), PBS, and cell culture medium (RPMI 1640 supplemented with 10% FBS) at 37°C. At predetermined time points (0, 6, 12, 18, and 24 h), aliquots were withdrawn, diluted with DW, and subjected to size measurement by using DLS.

In vitro drug release study

The in vitro drug release study of the DTX-loaded formulations was performed by using a dialysis bag diffusion method.[21] Briefly, 1 mL of DTX-Sol, DTX-NLC, or DTX-RIPL-NLC was placed in a dialysis bag (50 kDa MWCO, Biotech CE Tubing; Spectrum Laboratories, Inc., Rancho Dominguez, CA, USA). The dialysis bag was clipped by using a closer and soaked in a beaker containing 50 mL of release medium (0.5% sodium dodecyl sulfate in PBS, pH 7.4) to achieve sink conditions. Beakers were sealed with parafilm and maintained at 37°C with gentle stirring with a magnetic bar at 100 rpm. At predetermined time points, aliquots (0.5 mL) were withdrawn from the beaker and replaced with an equal volume of fresh release medium. The aliquots were analyzed by HPLC as described above.

Cell culture

Human ovarian carcinoma (SKOV3) and human prostate cancer cell lines (LNCaP, PC-3 and DU145) were grown in RPMI 1640 medium. In all cases, the medium was supplemented with 10% FBS, 100 units/mL penicillin G, and 100 μg/mL streptomycin. The cell lines were grown at 70%–80% confluence and maintained at 37°C in a humidified 5% CO_2 incubator. The cells were subcultured every 2–4 days and were used for experiments at passages 5–20.

In vitro cellular uptake study of NLC formulations

For the cellular uptake study, DiI was loaded to NLC dispersions instead of DTX at a concentration of 10 μg/mL. The cellular uptake behaviors of DiI-loaded NLC (DiI-NLC) and DiI-loaded RIPL-NLC (DiI-RIPL-NLC) were evaluated on SKOV3, MCF7, PC-3, and DU145 cells. For qualitative analysis, cells were seeded in a chambered coverglass (Thermo Scientific Nunc) at a density of 1×10^4 cells per well and incubated for 24 h at 37°C. After 24 h, the cells were washed with PBS twice. Then, the media were placed into serum-free media with DiI solution, DiI-NLC, or DiI-RIPL-NLC, in which the concentration of DiI was 100 ng/mL. Following 2 h of incubation, the cells were washed three times. Finally,

the cells were observed by using a fluorescence microscope (Motic, Beijing, China) under 40× magnification.

For the quantitative analysis of intracellular delivery of the DiI-NLC, cells were seeded into a six-well plate at a density of 3×10^5 cells per well. After 24 h of incubation, the medium was removed, and the cells were washed twice with PBS and replaced with serum-free medium. Then, the cells were incubated for 2 h at 37°C in media (2 mL) with formulations containing equivalent amounts of DiI (200 ng). Subsequently, the cells were washed three times with PBS, harvested by trypsin-EDTA, and suspended in PBS (1 mL). The cell suspensions were introduced into a flow cytometer (FACSCalibur; Becton Dickinson, Franklin Lakes, NJ, USA) equipped with a 488-nm argon-ion laser. Cell-associated fluorescence was quantitatively determined by flow cytometer by counting 10,000 events detected in the FL2 channel. Only the viable cells were gated for fluorescence analysis. All experiments were performed in triplicate.

Observation of translocational behavior

The translocational behavior of DiI-RIPL-NLC into cultured cells was visualized by using confocal laser scanning microscopy (Zeiss LSM 700 Meta confocal microscope; Carl Zeiss Meditec AG, Jena, Germany). SKOV3 and PC-3 cells were seeded on NUNC CC2 glass slides (Thermo Scientific Nunc) at a density of 5×10^4 cells/well and incubated for 24 h at 37°C. Cells were incubated with DiI-RIPL-NLC for predetermined time periods: 0 (immediately after the treatment), 1, 2, and 4 h. Following incubation, the cells were washed three times with PBS and fixed with 4% formaldehyde in PBS for 15 min at room temperature. The cells were mounted by using Vectashield mounting medium containing DAPI (H-1200) to stain the nuclei and avoid fading. The images were obtained by using the Z-stacking mode (z 1-11, slice thickness 10 µm) under 400× magnification.

Cytotoxicity assessment

The cytotoxicity of both DTX-free and DTX-loaded NLC formulations against SKOV3, LNCaP, PC-3, and DU145 cells was measured by WST-1 assay. Cells were seeded into a 96-well plate at a density of 1×10^4 cells per well and allowed to adhere for 24 h prior to the assay. Then, the cells were incubated at 37°C for 24 h with culture medium containing empty formulations (DTX-free) or DTX-loaded formulation at concentrations of 0.1, 1, 10, 100, 500, and 1,000 ng/mL as DTX equivalent. Culture medium was used as a blank control. Next, cells were incubated with 10% WST-1 reagent

at 37°C for 30 min. The absorbance of WST formazan dye was assessed at 450 nm by using a microplate reader (Flex station 3; Molecular Devices LLC, Sunnyvale, CA, USA). Cell viability was determined as the percentage of viable cells relative to the blank control.

In vivo TGI study

The in vivo TGI study was examined in a SKOV3 cell xenograft mouse model.[22] The female BALB/c athymic mice (5–6 weeks, 20±2 g) were subcutaneously injected in the right flank with 100 µL of RPMI 1640/Matrigel (50:50 v/v) suspension containing 2×10^6 SKOV3 cells. Digital calipers (Mitutoyo, Kawasaki, Japan) were used to measure the tumor dimensions.[23] The tumor volume was calculated by using the following equation: tumor volume (mm^3) = 1/2 × length × width × height.[24] When the tumor volume reached about 130 mm^3, the mice were divided into four groups: 1) 0.9% saline solution-treated (Control), 2) DTX-Sol, 3) DTX-NLC, and 4) DTX-RIPL-NLC. The mice in each group received 10 mg/kg DTX intratumorally by using a 21 G gauge needle once per week for 3 weeks. The injection volume was 100 µL, and the first day of administration was designated as day 0. Tumor volumes and the body weights of the mice were measured weekly for 6 weeks. The general health status of mice was also documented including potential side effects, food avoidance, and behavioral changes. At the end of the experiment, the mice were sacrificed by cervical dislocation, and the tumors excised free of skin and tissues, and then weighed and photographed. The antitumor efficacy of each formulation was evaluated by the ratio of TGI, which was calculated by using the following equation:[17]

$$\text{TGI (\%)} = \left(1 - \frac{W_t}{W_c}\right) \times 100$$

where W_t and W_c represent the tumor weight for the treated and control group, respectively.

Statistical analysis

Values are presented as mean ± standard deviation (n=3). Statistical significance was determined by Student's t-tests and considered to be significant at $P<0.05$.

Results and discussion

Physicochemical characterization of NLCs

The physical characteristics of various NLCs were evaluated in terms of particle size, size distribution (polydispersity

Table 1 Physicochemical characteristics of NLCs

Characteristics	NLC	RIPL-NLC
Drug-free		
Size (nm)	154.63±6.15	232.57±26.26
PDI	0.270	0.294
Zeta potential (mV)	−16.31±0.44	19.7±0.41
DiI-loaded		
Size (nm)	166.93±8.30	269.63±7.92
PDI	0.232	0.319
Zeta potential (mV)	−15.23±0.71	23.80±2.03
DTX-loaded		
Size (nm)	184.73±6.48	240.83±3.44
PDI	0.193	0.265
Zeta potential (mV)	−24.03±0.26	14.27±0.78
Encapsulation efficiency (%)	94.89±0.21	97.59±0.13
Drug loading (µg/mg)	44.2±0.10	45.9±0.20

Note: Data represent mean ± SD (n=3).
Abbreviations: DiI, 1,1′-dioctadecyl-3,3,3′,3′-tetramethylindocarbocyanine perchlorate; DTX, docetaxel; NLCs, nanostructured lipid carriers; PDI, polydispersity index; RIPL-NLC, RIPL peptide-conjugated NLC.

index, PDI), ZP, EE, and DL (Table 1). The average sizes of all NLCs were observed in the range of 150–250 nm by DLS. Polydispersity was below 0.3, indicating a narrow and homogeneous size distribution. There were no changes in nanodispersion characteristics until use in the experiment. The particle size was slightly increased by encapsulation of molecules (DiI or DTX) compared to the drug-free NLCs. The conjugation of RIPL peptides onto maleimide-derivatized NLCs resulted in an increase of particle size to about 250 nm. However, EE (%) and DL (µg/mg) were not critically affected by RIPL modification: 94.9% and 44.2 µg/mg for NLC; 97.6% and 45.9 µg/mg for RIPL-NLC, respectively. These values were comparable with those of similar NLC systems reported elsewhere,[25,26] but significantly higher than those of liposomal systems. In our earlier study, liposomal encapsulation of DTX has been extremely limited, resulting in poor EE and DL (35% and 22 µg/mg in average).[17] In terms of ZP, all NLCs and maleimide-derivatized NLCs showed negative charge, whereas RIPL-NLC, RIPL-DiI-NLC, and DTX-RIPL-NLC were positively charged with a ZP value of about 20, 24, and 14 mV, respectively. Changes in ZP indicated that the positively charged RIPL peptide was attached onto the maleimide-derivatized NLCs.

To confirm the conjugation of the RIPL peptides on the NLC surfaces, unreacted RIPL peptides were analyzed (Figure 2A). Unlike the liposome systems in which ~50% of maleimide groups were externally oriented,[12] maleimide groups were mostly externally placed in this NLC system, providing favorable conditions for further modification.

The degree of RIPL conjugation increased as time passed and reached a plateau at 12 h, indicating the completion of the conjugation reaction. Due to this surface modification, as shown in Figure 2B, the calculated FALT value of RIPL-NLC (2.87±2.74 nm) was 1.8-fold greater than that of NLC, suggesting a mushroom-like structure of the poly-(ethylene glycol) (PEG) layer.[27] The TEM images revealed that DTX-NLC and DTX-RIPL-NLC were spherical in morphology (Figure 2C). The diameters of the nanocarriers observed in the TEM images corroborate with the particle size measured by Zetasizer. DSC has been used to examine the crystallization and the melting behavior of crystalline material.[28] Figure 2D shows DSC curves for DTX, DTX-loaded NLCs, and Precirol® ATO 5 as a solid lipid of NLC. DTX only exhibited an endothermic peak at 164.96°C, while Precirol® ATO 5 exhibited the peak at 58.26°C, as similarly reported in the literature.[29,30] Although there was a trace of peak shift to the lower temperature, DTX-NLC and DTX-RIPL-NLC did not present the typical endothermic peak of DTX, indicating that DTX was entrapped into the innermost compartment of the NLCs.

The size and PDI of nanocarriers play an important role in their distribution in vivo and in their intracellular transport.[31] Solid tumors show increased permeability and impaired lymphatic drainage which is well-known as the "enhanced permeability and retention (EPR)" effect.[32] Nanocarriers that have a size below 500 nm may exploit this abnormality of the tumor to accumulate in the tumor across the enlarged gap junctions which are between 100 and 780 nm in size.[33,34] It is also beneficial for nanocarriers to have an optimal size and spherical morphology to be internalized. Compared to rod-shaped particles, spherical particles can be taken up more easily by cancer cells due to the shorter membrane wrapping time for internalization.[35] Therefore, spherically shaped RIPL-NLCs with a size of around 250 nm and a PDI of 0.3 are considered desirable as the optimized formulation for in vitro and in vivo experiments. Figure 3 shows the colloidal dispersion stability of DTX-NLC and DTX-RIPL-NLC in different media such as DW, PBS, and cell culture medium (RPMI 1640 supplemented with 10% FBS). Regardless of the media type, any significant changes in particle size were not observed for 24 h, indicating that both NLCs were physically stable against in vitro and in vivo circumstances. The ZP of nanocarriers, which is a sign of the strength of the attractive and repulsive forces between nanocarriers, is a key factor in the evaluation of the stability of colloidal carrier systems.[36] In general, the more over 15 mV the absolute ZP value is, the stronger the electrostatic repulsion between the particles.[37]
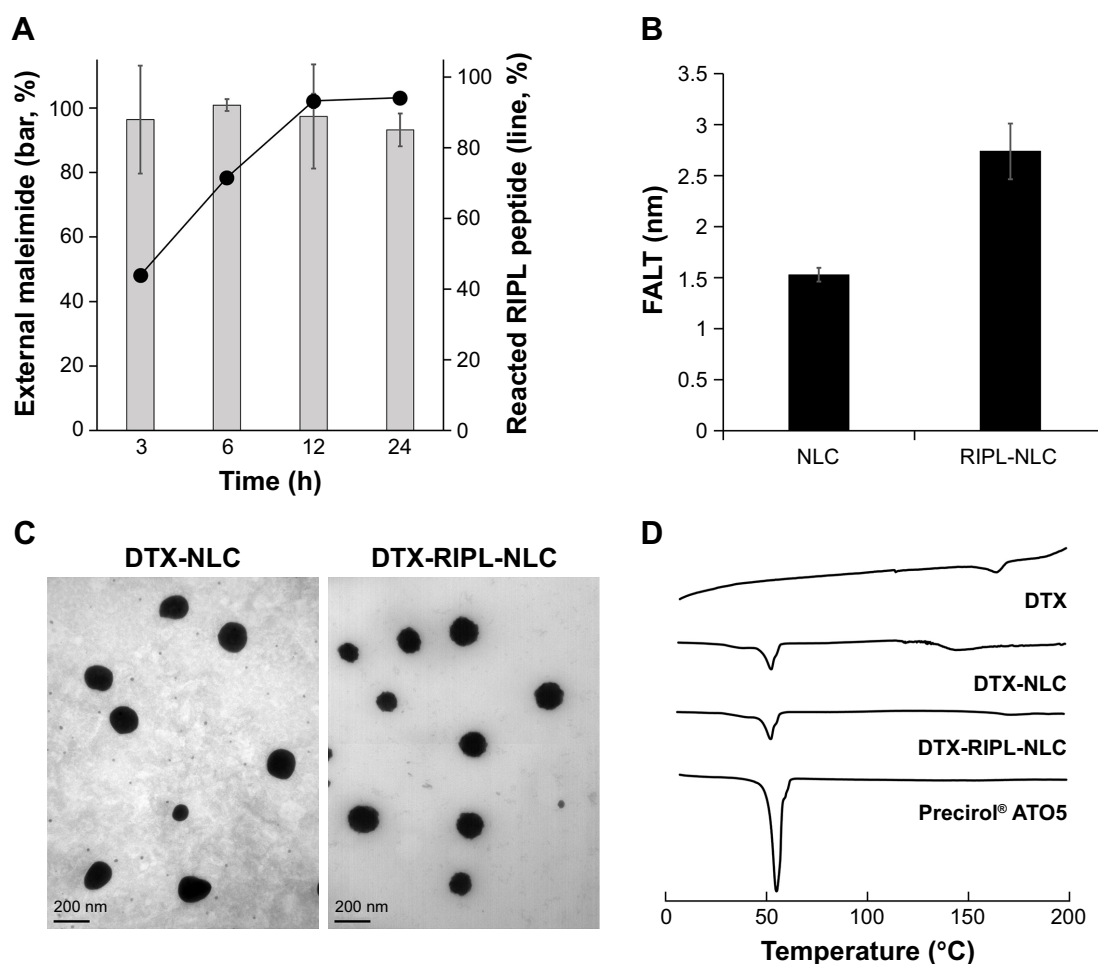
Figure 2 Characterization of RIPL-NLC.
Notes: (**A**) Time-dependency of the thiol-maleimide reaction. (**B**) Comparison of the calculated FALT of NLC and RIPL-NLC. (**C**) TEM images of DTX-NLC and DTX-RIPL-NLC. (**D**) DSC thermograms of DTX, Precirol® ATO 5, DTX-NLC, and DTX-RIPL-NLC. Data are mean ± SD (n=3).
Abbreviations: DSC, differential scanning calorimetry; DTX-NLC, DTX-loaded nanostructured lipid carrier; DTX-RIPL-NLC, docetaxel-loaded RIPL peptide-conjugated nanostructured lipid carrier; FALT, fixed aqueous layer thickness; NLC, nanostructured lipid carrier; RIPL-NLC, RIPL peptide-conjugated nanostructured lipid carrier; TEM, transmission electron microscopy.
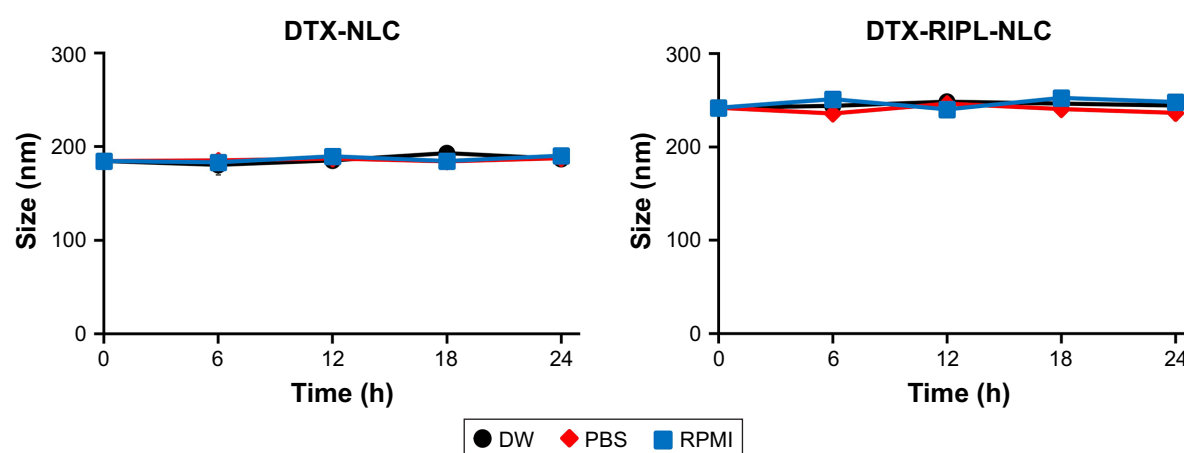
Figure 3 Colloidal stability of DTX-loaded NLCs in different media.
Notes: Samples were incubated at 37°C. Particle size was determined by dynamic light scattering. Data are mean ± SD (n=3).
Abbreviations: DTX, docetaxel; DW, distilled water; PBS, phosphate-buffered saline; RPMI, Roswell Park Memorial Institute 1640 medium; DTX-NLC, docetaxel-loaded nanostructured lipid carrier; DTX-RIPL-NLC, docetaxel-loaded RIPL peptide-conjugated nanostructured lipid carrier.

All the NLCs and RIPL-NLCs exhibited an absolute ZP value above 15 mV, indicating that these particles could remain stable during storage without aggregation between NLC particles, due to their electrostatic repulsion. Furthermore, since the plasma membrane of cells exhibits negatively charged characteristics, positively charged nanocarriers would efficiently interact with the plasma membrane, resulting in a greater chance to be internalized.[38]

In vitro drug release profile

The in vitro release of DTX from different samples of DTX-Sol, DTX-NLC, and DTX-RIPL-NLC was evaluated by using a dialysis bag diffusion method under sink conditions (Figure 4). DTX release from DTX-Sol reached ~90% within 6 h, whereas the release from DTX-NLC and DTX-RIPL-NLC was about 33% and 14%, respectively, for the same time period. Compared to the fast release of DTX-Sol, DTX-NLC and DTX-RIPL-NLC showed a prolonged and sustained drug release pattern, with a fast release in the initial period of 6 h, followed by a sustained release for up to 60 h. The initial rapid release of DTX-loaded NLCs may be caused by the enrichment of DTX in the outer surface of the NLCs that immediately diffuses into the release medium.[39] The later sustained release could be attributed to the degradation and erosion of the inner lipid matrix where the drug could be molecularly dispersed or dissolved.[40] This release pattern would be beneficial for clinical anticancer therapy by reducing the frequency of administration.
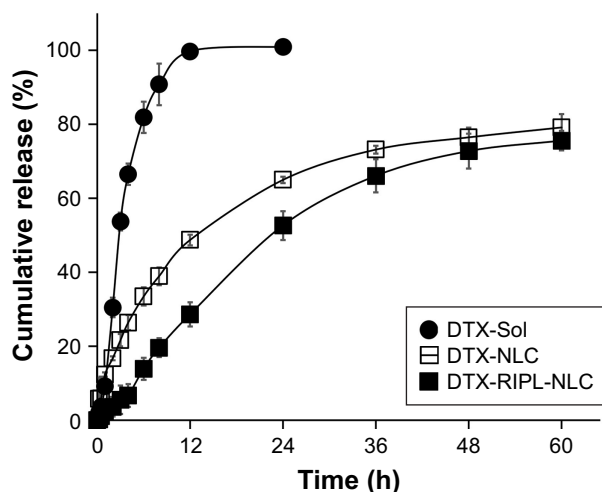
The drug release mechanism was further determined by fitting the release profile data to release kinetic models, such as zero-order, first-order, and Higuchi equations.[41] As shown in Table 2, DTX-Sol was fitted to the first-order equation, whereas DTX-NLC and DTX-RIPL-NLC were fitted to the Higuchi equation.[42,43] Thus, we assumed that the NLCs had a matrix-type structure in which DTX was homogeneously dispersed throughout the matrix and that the release was diffusion-controlled.[44] Particularly, the release rate constant of DTX-RIPL-NLC was slightly reduced compared to that of DTX-NLC. This is probably due to the release mechanism of diffusion, specifically in terms of diffusional path length. First, the FALT value of DTX-RIPL-NLC was greater than that of DTX-NLC, indicating a barrier for diffusion. In addition, as PEG chains and RIPL peptides are hydrated upon exposure to the release medium, FALT becomes larger, thus increasing the diffusion distance which results in slower release.[45]

In vitro cellular uptake evaluation of DiI-RIPL-NLCs

To evaluate the target-selective uptake behavior of NLCs, various cells (SKOV3, LNCaP, DU145, and PC-3) were treated with DiI-loaded formulations. The cells were visualized by fluorescence microscopy after 2 h of incubation (Figure 5A). Red fluorescence spots were rarely observed in cells incubated with DiI solution, regardless of cell type. In the case of DiI-NLC, red fluorescence with weak intensity was observed in the vicinity of the cell membranes. In contrast, the red fluorescence intensity of DiI-RIPL-NLC-treated cells was significantly stronger than the other formulations and depended on Hpn expression; abundant red fluorescence was visible in Hpn(+) cells, while only weak spots were visible in Hpn(−) cells. This indicates that the surface modification with the RIPL peptide displayed

Figure 4 In vitro drug release profile of various DTX formulations.
Note: Data are mean ± SD (n=3).
Abbreviations: DTX, docetaxel; DTX-Sol, docetaxel solution; DTX-NLC, docetaxel-loaded nanostructured lipid carrier; DTX-RIPL-NLC, docetaxel-loaded RIPL peptide-conjugated nanostructured lipid carrier.

Table 2 In vitro release kinetic parameters of various DTX formulations

Formulations	Zero-order		First-order		Higuchi model	
	r^2	K_0	r^2	K_1	r^2	K_H
DTX-Sol	0.8701	9.3674	0.9101	0.2036	0.8620	26.632
DTX-NLC	0.8320	1.2983	0.9772	0.0477	0.9797	11.979
DTX-RIPL-NLC	0.9381	1.4246	0.9725	0.0297	0.9764	11.833

Notes: K_0, zero-order rate constant; K_1, first-order rate constant; K_H, Higuchi equation's rate constant; r^2, correlation coefficient.
Abbreviations: DTX, docetaxel; DTX-Sol, docetaxel solution; DTX-NLC, docetaxel-loaded nanostructured lipid carrier; DTX-RIPL-NLC, docetaxel-loaded RIPL peptide-conjugated nanostructured lipid carrier.

a better selective binding affinity of the nanocarrier to the extracellular membrane of Hpn(+) cells.

Further quantification of the cellular uptake of NLCs by RIPL peptide modification was evaluated by flow cytometry using the same cancer cell lines. Cells were again incubated with the different DiI-loaded formulations for 2 h at 37°C.

A low level of background fluorescence was observed in untreated cells. As shown in Figure 5B, little or no shift of the fluorescence peak was observed in any of the cell lines between the DiI-NLC and DiI solution treatments. However, a great shift of the peak was observed for the DiI-RIPL-NLC treatment, specifically for Hpn(+) cells. The relative mean
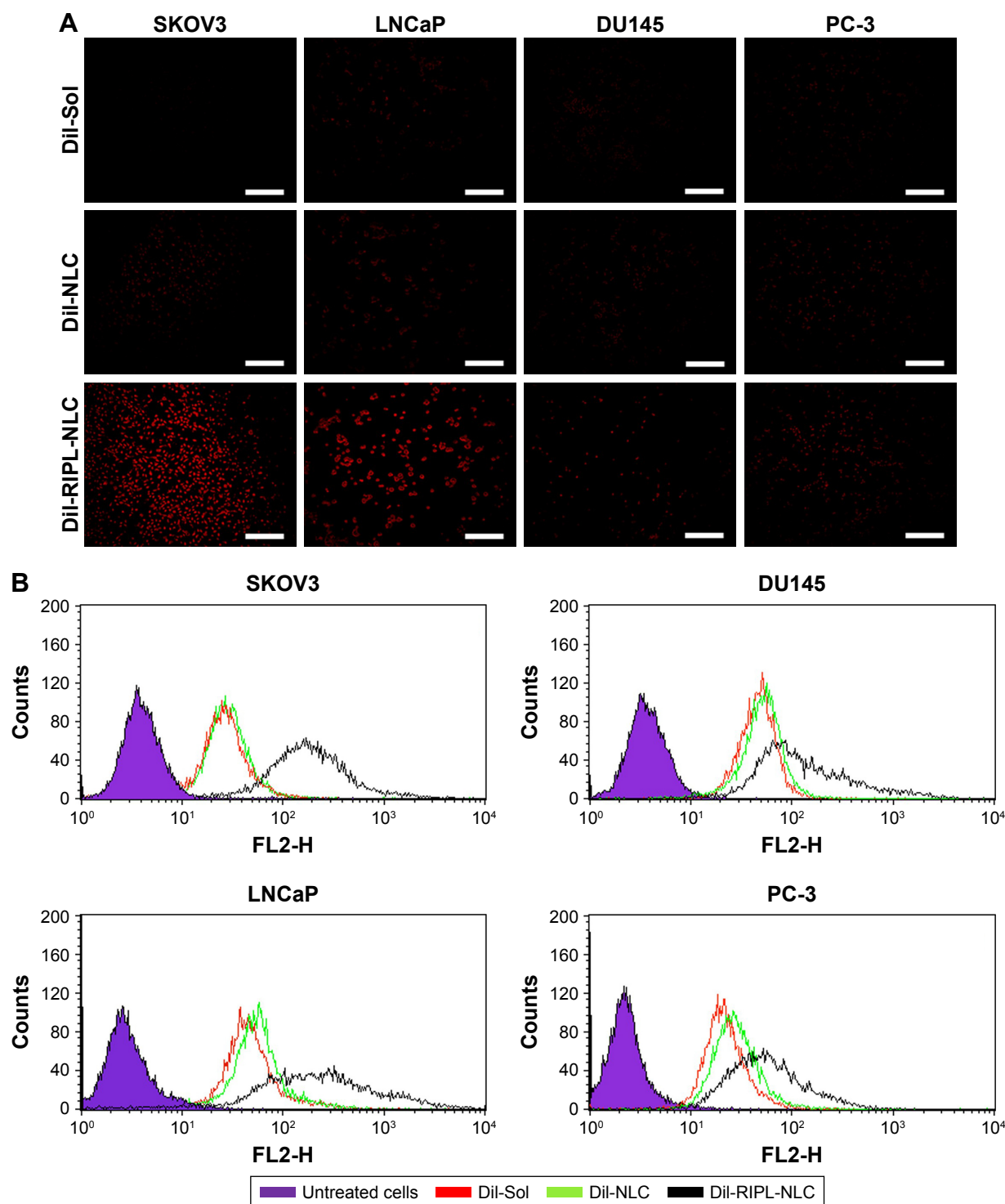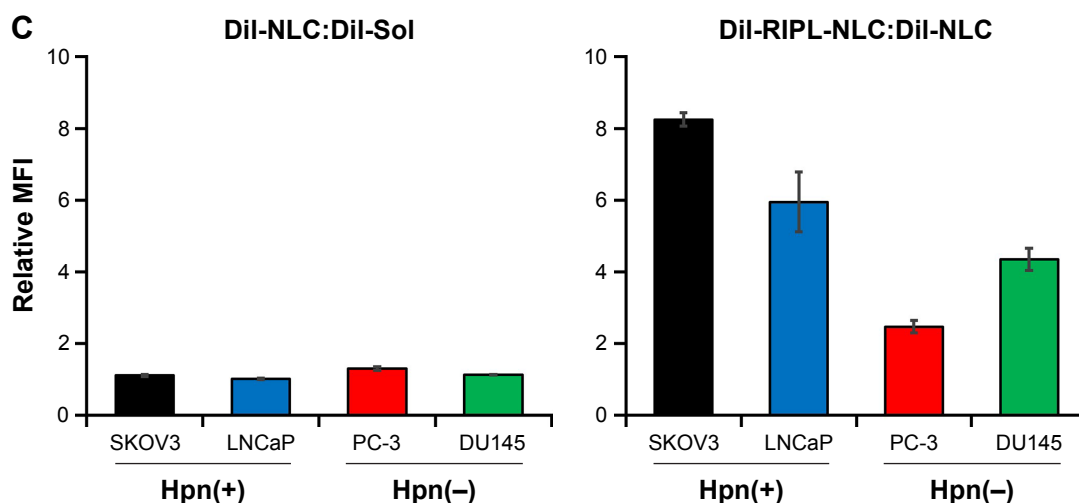

Figure 5 (*Continued*)

C

Figure 5 The qualitative and quantitative analysis of the cellular uptake of DiI-loaded formulations.
Notes: (**A**) Fluorescence microscopy images of various cell lines incubated with DiI-Sol, DiI-NLC, and DiI-RIPL-NLC at 37°C for 2 h. Concentration of DiI was 200 ng/mL. White scale bar represents 100 μm. (**B**) Flow cytometry histogram shows the treatment effect: untreated cells (purple); cells treated with DiI-Sol (red), DiI-NLC (green), and DiI-RIPL-NLC (black). (**C**) The relative ratio of MFI values in different treatments: DiI-NLC versus DiI-Sol; DiI-RIPL-NLC versus DiI-NLC. Data are mean ± SD (n=3).
Abbreviations: DiI, 1,1′-dioctadecyl-3,3,3′,3′-tetramethylindocarbocyanine perchlorate; DiI-Sol, DiI solution; DiI-NLC, DiI-loaded nanostructured lipid carrier; DiI-RIPL-NLC, DiI-loaded RIPL peptide-conjugated nanostructured lipid carrier; Hpn, Hepsin; MFI, mean fluorescence intensity.

fluorescence intensity (MFI) values indicated that DiI-NLC increased the uptake degree less than 1.3-fold compared to the DiI solution (Figure 5C). However, compared to DiI-NLC, DiI-RIPL-NLC showed 8.3- and 6.2-fold increases in Hpn(+) cells (SKOV3 and LNCaP) and ~2.5- and 4.3-fold increases in Hpn(−) cells (PC-3 and DU145). The cellular uptake of DiI, a lipophilic molecule, was increased by NLC formulation and further enhanced by modifying the NLC surface with RIPL peptide. As a CPHP, RIPL peptide is composed of a Hpn-recognizing sequence (IPLVVPL) and a cell-penetration enhancing sequence (octaarginine; R_8). In Hpn(+) cells, cellular uptake of DiI-RIPL-NLC was higher than that in Hpn(−) cells due to the synergistic effect of both the domains of the RIPL peptide. Meanwhile, RIPL peptide also increased the fluorescence intensity of DiI-RIPL-NLC compared to DiI-NLC in Hpn(−) cells. This non-specific uptake could be caused by the cell-penetrating function of the R_8 sequence in the RIPL peptide.

Assessment of translocational behavior of RIPL-NLCs

Based on the strongest fluorescence intensity in the fluorescence microscopy images and the highest MFI values in the cellular uptake study by flow cytometry, the translocational behavior of RIPL-NLC was further investigated in SKOV3 and PC-3 cell lines by confocal microscopy with orthogonal views (Figure 6). Cells were seeded on glass slides and incubated with DiI-RIPL-NLC for predetermined time periods after treatment. Immediately after the treatment

with DiI-RIPL-NLC, no fluorescence was observed in the cell membranes of both the cell lines. Afterward, as expected, intracellular translocation was Hpn-specific and time-dependent: after 1 h, weak red fluorescence appeared in the cytosol, but the intensity became significantly different between Hpn(+) and Hpn(−) cells; after 2 h, the fluorescence in the cytosol was increased overall and reached maximum intensity, revealing the greatest difference between the two cells; after 4 h, fluorescence intensity was maintained, revealing the scattered dot-like fluorescence throughout the cytoplasm. Specifically in Hpn(+) SKOV3 cells, red fluorescence with strong intensity was observed in the interior compartment of the cell and distributed throughout the cell structure, confirming DiI-RIPL-NLC internalization into the cells. After 2 h, in all orthogonal planes, red fluorescence became strengthened and appeared to spread out radially with increased intensity as time passed.

Z-stacking images confirm that DiI-RIPL-NLCs not only bound to the surface of Hpn-expressing SKOV3 cells but was also internalized across the cellular membrane into the cytoplasm. The fluorescent intensity of the DAPI-stained nuclei has been maintained throughout the experiment, but that of the DiI was weak for the first 1 h. This indicates that there was no premature DiI release from the DiI-RIPL-NLC in the extracellular region, in which DiI can rapidly diffuse into the cytoplasm. As the cytosolic internalization of DiI-RIPL-NLC was time-dependent, it can be concluded that the RIPL peptide enhanced the translocation of NLC by the internalization mechanisms of polyarginine such as direct
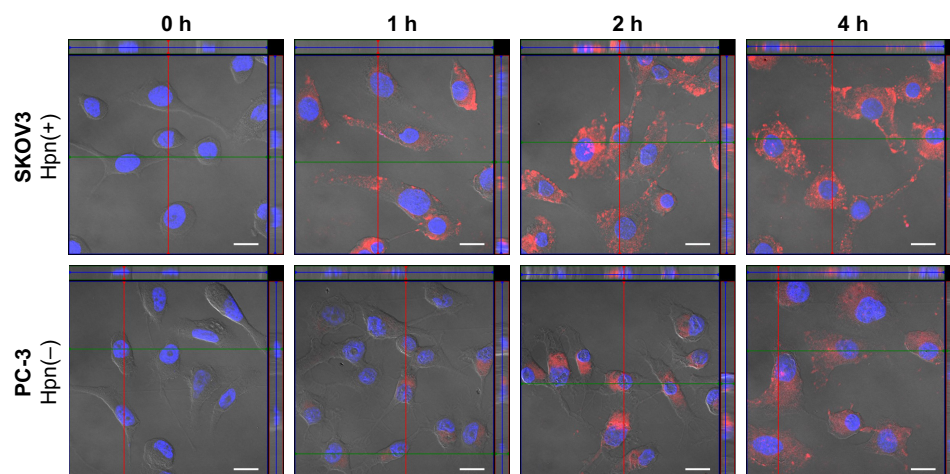
Figure 6 Confocal microscopic images with orthogonal views of SKOV3 and PC-3 cells.
Notes: Cells incubated with DiI-RIPL-NLC for 0 (immediately after the treatment), 1, 2, and 4 h. The nucleus was stained with DAPI for blue fluorescence and merged with red fluorescence of DiI distributed in the cytoplasm. The positions of the section plane are indicated by colored lines; XY plane (blue), XZ plane (green), YZ plane (red). The white scale bar represents 20 µm.
Abbreviations: DAPI, 4′,6-diamino-2-phenylindole; DiI, 1,1′-dioctadecyl-3,3,3′,3′-tetramethylindocarbocyanine perchlorate; DiI-Sol, DiI solution; DiI-NLC, DiI-loaded nanostructured lipid carrier; DiI-RIPL-NLC, DiI-loaded RIPL peptide-conjugated nanostructured lipid carrier; Hpn, hepsin.

penetration or macropinocytosis.[46,47] In addition, DiI-RIPL-NLC was internalized into the intracellular region after exposure to SKOV3 cells for a relatively short period of time. This observation supports the flow cytometry results, indicating that DiI-RIPL-NLC selectively binds to Hpn-expressing cells and enhances cellular uptake.

Cytotoxicity of drug-free and DTX-loaded formulations

The toxicities of drug-free and DTX-loaded formulations were examined by using SKOV3, LNCaP, DU145, and PC-3 cells for 24 h (Figure 7). The cells were treated with variable concentrations of DTX, and cell viability was examined
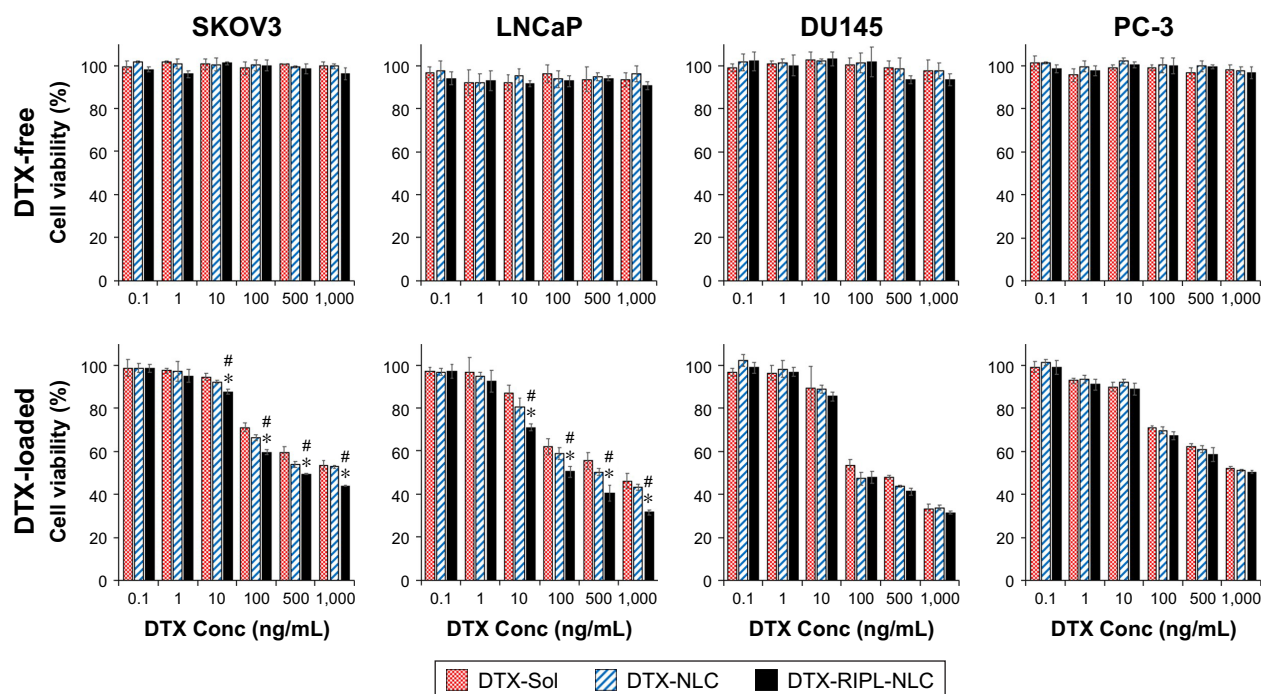

Figure 7 The cytotoxicity of DTX-free formulations (upper panels) and DTX-loaded formulations (lower panels) on SKOV3, LNCaP, DU145, and PC-3 cells by WST-1 assay.
Notes: Data are mean ± SD (n=3). Statistical analysis was performed by using Student's t-test (*$P<0.05$ versus DTX-Sol; #$P<0.05$ versus DTX-NLC).
Abbreviations: DTX, docetaxel; DTX-Sol, docetaxel solution; DTX-NLC, docetaxel-loaded nanostructured lipid carrier; DTX-RIPL-NLC, docetaxel-loaded RIPL peptide-conjugated nanostructured lipid carrier; Conc, concentration.

by WST-1 assay. Cell viability in the untreated group was considered as 100%. All drug-free formulations revealed no significant cell death in the concentration range used in this experiment (Figure 7, upper panel), whereas DTX-loaded formulations showed dose-dependent, but different, results depending on Hpn(+) and Hpn(−) cells (lower panel). There were no significant differences in cytotoxicity associated with the RIPL modification in Hpn(−) cells. Comparatively, in the Hpn(+) cells, RIPL-DTX-NLC showed significantly stronger cytotoxicity than DTX-NLC and DTX-Sol, regardless of DTX concentration. A possible mechanism underlying the lower cell viability of RIPL-DTX-NLC-treated cells may include the enhanced intracellular DTX accumulation due to CPHP-modified nanocarrier uptake. These results are consistent with other cellular uptake studies, as described above, and a paper suggesting that the strongest antiproliferation effect on cancer cells was induced by the conjugation of CPHP on the surface of a liposome.[48]

In vivo TGI study

Antitumor efficacy was evaluated by measuring tumor volume and body weight changes after intratumoral injections of different DTX formulations. Based on the cellular uptake and cytotoxicity studies, a SKOV3 xenograft model was selected for the in vivo TGI study. In this experiment, intratumoral injections were adopted instead of intravenous administration, because sufficient and accurate concentrations of drug could be exposed to the local tumor tissue upon intratumoral injection.[49] NLC samples of either DTX-RIPL-NLC or DTX-NLC, and reference samples of either DTX-Sol (positive control) or saline (negative control) were used in each mouse. Samples were intratumorally injected with three consecutive doses, that is, the first dose when the tumor volume reached approximately 130 mm^3, the second dose at day 7, and the final dose at day 14. For the first 2 weeks, as shown in Figure 8A, tumor volume showed little increase in the DTX-treated groups, but an ~2.5-fold increase in the saline-treated group by day 14, although the difference was statistically insignificant ($P<0.05$). However, a week after the last injection (day 21), significant changes were found. All DTX treatments were effective in preventing tumor growth. Specifically, the NLC-treated groups showed significant differences compared with the saline-treated group, and the differences were further increased by time. Finally, at the
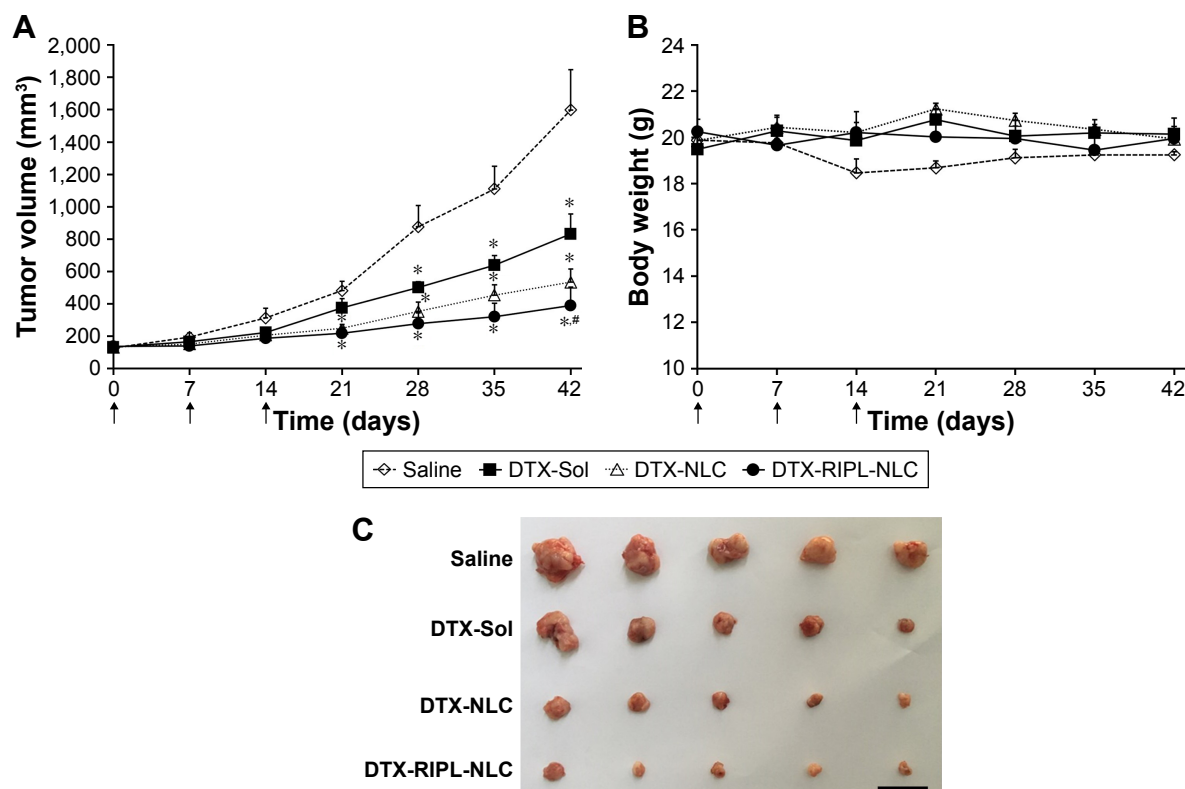

Figure 8 In vivo antitumor efficacies in SKOV3-bearing BALB/c nude mice treated with different formulations.
Notes: Animals (n=5) received 10 mg DTX/kg intratumorally on day 0, 7, and 14, a total of three injections per mouse as indicated by arrows. (**A**) Changes in tumor volume for 6 weeks post-administration. (**B**) Body weight changes for 6 weeks post-administration. (**C**) Morphology of excised xenograft tumors at the end of the study (day 42). Black bar indicates 30 mm. Statistical analysis was performed using Student's *t*-test (*$P<0.05$ versus saline; #$P<0.05$ versus DTX-Sol).
Abbreviations: DTX, docetaxel; DTX-Sol, docetaxel solution; DTX-NLC, docetaxel-loaded nanostructured lipid carrier; DTX-RIPL-NLC, docetaxel-loaded RIPL peptide-conjugated nanostructured lipid carrier.

termination of the experiment (day 42), the DTX-RIPL-NLC group exhibited the greatest TGI compared with the DTX-Sol or DTX-NLC groups.

As shown in Figure 8B, there were no significant weight changes in any group for 6 weeks, except for the saline-treated group which revealed a little weight loss in weeks 2–4. In general, a change of body weight reflects systemic toxicity.[50] As none of the DTX-treated animals showed acute body weight loss during the experiments, it could be concluded that there was no obvious side effect of the DTX-loaded formulations. However, considering that the body weight of xenografted animals tends to increase with time due to inherent body growth and increased tumor volume, the mice in the DTX-Sol-treated group were possibly subjected to "tumor-borne lean body" where their body weight gradually decreases with time, while the tumor grows substantially.[17] For further comparison, mice were sacrificed at the end of the experiment, and the excised tumors were photographed to provide a visual comparison of antitumor effects (Figure 8C). Tumor growth was suppressed greatly by the DTX treatments. The average tumor weights of the saline, DTX-Sol, DTX-NLC, and DTX-RIPL-NLC groups are listed in Table 3. The relative weight ratios of tumors were expressed as TGI percentages. The DTX-RIPL-NLC-treated tumors showed a TGI of 91.2%, which was significantly higher than that of DTX-NLC (86.9%) and DTX-Sol (61.4%)-treated tumors. Although all animals in each treatment group survived throughout the experiment, behavioral differences were remarkable. Mice in the saline group showed severe impaired movement with a hunched posture, a loss of activity, reddening and dried skin, and labored breathing. Mice with DTX-Sol treatment showed limited movement, a loss of appetite, and breathing difficulties. Unlike the two control groups, DTX-loaded NLC formulation groups showed a relatively improved quality of life with free movement and normal appetite.

As a result, DTX-RIPL-NLC showed higher antitumor efficacy and fewer side effects than DTX-Sol in the SKOV3-bearing mouse model, revealing consistency with the in vitro cytotoxicity observations. The significantly higher antitumor efficacy of DTX-RIPL-NLC could be attributed to the following mechanisms. First, the nanocarrier systems could convey several advantages, including the extended retention and sustained release of DTX in the tumors after intralesional administration. It is generally understood that chemotherapeutic agents with low molecular weights are not retained at the administered site, but diffuse rapidly into the blood's circulation.[51] Particulate carriers can extend their retention time, provide a sustained drug release, and result in enhanced antitumor efficacy.[34] In a previous study, improved antitumor efficacy with about 60% retardation in tumor growth for 15 days was observed after the intratumoral administration of paclitaxel/tetrandrine-coloaded nanoparticles.[52] Second, by virtue of the active role of RIPL peptide in targeting and internalization, RIPL-DTX-NLC could selectively bind to Hpn-expressing cancer cells and enhance the intracellular delivery of DTX. In earlier studies, we reported the usefulness of RIPL peptide as a CPHP by liposomal surface modification: RIPL-modified liposomes containing DTX significantly inhibited tumor growth and prolonged survival time in BALB/c nude mice with SKOV3 cell tumors.[17] Third, electrostatic interactions might be involved. Positively charged DTX-RIPL-NLC could efficiently bind to the negatively charged tumor surface due to interstitial components such as proteoglycans and glycocalyx.[53] In addition, cationic macromolecules have been found to largely remain in the tumor region compared to anionic macromolecules.[54] However, additional future studies on steric stabilization via PEGylation and on in vivo biodistribution after intravenous administration are still needed to develop a practical formulation.

Conclusion

RIPL-NLCs, encapsulating DTX in high loading capacity, were successfully developed for targeted delivery to Hpn-expressing cancer cells. Drug release was diffusion-controlled, and in vitro cytotoxicity was dose-dependent. RIPL-NLCs showed high target-selectivity and time-dependent translocation behavior into the cytoplasm. Moreover, in a SKOV3-bearing xenograft mouse model, DTX-RIPL-NLC significantly inhibited tumor growth. Therefore, DTX-RIPL-NLC would be a good candidate for Hpn-selective drug targeting.

Acknowledgment

Table 3 Antitumor efficacy of treatment groups in a SKOV3 cell-bearing xenograft mouse model

Treatment group	Dose (mg/kg)	Number of animals (start/end)	Average tumor weight (g)	TGI (%)
Saline	–	5/5	3.53±1.46	–
DTX-Sol	10	5/5	1.37±0.92*	61.39
DTX-NLC	10	5/5	0.46±0.28*	86.94
DTX-RIPL-NLC	10	5/5	0.31±0.15*,#	91.24

Notes: Data are mean ± SD (n=3). *$P<0.05$ versus saline; #$P<0.05$ versus DTX-Sol. **Abbreviations:** DTX-Sol, docetaxel solution; DTX-NLC, docetaxel-loaded nanostructured lipid carrier; DTX-RIPL-NLC, docetaxel-loaded RIPL peptide-conjugated nanostructured lipid carrier; TGI, tumor growth inhibition.

Disclosure

The authors report no conflicts of interest in this work.

References

1. Bertrand N, Wu J, Xu X, Kamaly N, Farokhzad OC. Cancer nanotechnology: the impact of passive and active targeting in the era of modern cancer biology. *Adv Drug Deliv Rev*. 2014;66:2–25.
2. Wang S, Zhao J, Yang H, et al. Bottom-up synthesis of WS2 nanosheets with synchronous surface modification for imaging guided tumor regression. *Acta Biomater*. 2017;58:442–454.
3. Tikekar RV, Nitin N. Distribution of encapsulated materials in colloidal particles and its impact on oxidative stability of encapsulated materials. *Langmuir*. 2012;28(25):9233–9243.
4. Müller RH, Petersen RD, Hommoss A, Pardeike J. Nanostructured lipid carriers (NLC) in cosmetic dermal products. *Adv Drug Deliv Rev*. 2007;59(6):522–530.
5. Üner M. Preparation, characterization and physico-chemical properties of solid lipid nanoparticles (SLN) and nanostructured lipid carriers (NLC): their benefits as colloidal drug carrier systems. *Pharmazie*. 2006;61(5):375–386.
6. Müller RH, Radtke M, Wissing SA. Nanostructured lipid matrices for improved microencapsulation of drugs. *Int J Pharm*. 2002;242(1–2):121–128.
7. Liu Y, Miyoshi H, Nakamura M. Nanomedicine for drug delivery and imaging: a promising avenue for cancer therapy and diagnosis using targeted functional nanoparticles. *Int J Cancer*. 2007;120(12):2527–2537.
8. Parveen S, Misra R, Sahoo SK. Nanoparticles: a boon to drug delivery, therapeutics, diagnostics and imaging. *Nanomedicine*. 2012;8(2):147–166.
9. Kim CH, Lee SG, Kang MJ, Lee S, Choi YW. Surface modification of lipid-based nanocarriers for cancer cell-specific drug targeting. *J Pharm Invest*. 2017;47(3):203–227.
10. Bugge TH, Antalis TM, Wu Q. Type II transmembrane serine proteases. *J Biol Chem*. 2009;284(35):23177–23181.
11. Kelly KA, Setlur SR, Ross R, et al. Detection of early prostate cancer using a hepsin-targeted imaging agent. *Cancer Res*. 2008;68(7):2286–2291.
12. Kang MH, Park MJ, Yoo HJ, et al. RIPL peptide (IPLVVPLRRRRRRRRC)-conjugated liposomes for enhanced intracellular drug delivery to hepsin-expressing cancer cells. *Eur J Pharm Biopharm*. 2014;87(3):489–499.
13. Vivès E, Schmidt J, Pèlegrin A. Cell-penetrating and cell-targeting peptides in drug delivery. *Biochim Biophys Acta*. 2008;1786(2):126–138.
14. Liu R, Li X, Xiao W, Lam KS. Tumor-targeting peptides from combinatorial libraries. *Adv Drug Deliv Rev*. 2017;110–111:13–37.
15. Sakurai Y, Kajimoto K, Harashima H. Anti-angiogenic nanotherapy via active targeting systems to tumors and adipose tissue vasculature. *Biomater Sci*. 2015;3(9):1253–1265.
16. Liu Y, Ran R, Chen J, et al. Paclitaxel loaded liposomes decorated with a multifunctional tandem peptide for glioma targeting. *Biomaterial*. 2014;35(17):4835–4847.
17. Yoon HY, Kwak SS, Jang MH, et al. Docetaxel-loaded RIPL peptide (IPLVVPLRRRRRRRRC)-conjugated liposomes: drug release, cytotoxicity, and antitumor efficacy. *Int J Pharm*. 2017;523(1):229–237.
18. Sadzuka Y, Nakade A, Hirama R, et al. Effects of mixed polyethyleneglycol modification on fixed aqueous layer thickness and antitumor activity of doxorubicin containing liposome. *Int J Pharm*. 2002;238(1):171–180.
19. Moser M, Behnke T, Hamers-Allin C, Klein-Hartwig K, Falkenhagen J, Resch-Genger U. Quantification of PEG-maleimide ligands and coupling efficiencies on nanoparticles with Ellman's reagent. *Anal Chem*. 2015;87(18):9376–9383.
20. Zhang B, Zhang Y, Yu D. Lung cancer gene therapy: transferrin and hyaluronic acid dual ligand-decorated novel lipid carriers for targeted gene delivery. *Oncol Rep*. 2017;37(2):937–944.
21. Shao Z, Shao J, Tan B, et al. Targeted lung cancer therapy: preparation and optimization of transferrin-decorated nanostructured lipid carriers as novel nanomedicine for co-delivery of anticancer drugs and DNA. *Int J Nanomedicine*. 2015;10:1223–1233.
22. Zheng D, Li D, Lu X, Feng Z. Enhanced antitumor efficiency of docetaxel-loaded nanoparticles in a human ovarian xenograft model with lower systemic toxicities by intratumoral delivery. *Oncol Rep*. 2010;23(3):717–724.
23. Wu C, Zhao J, Hu F, et al. Design of injectable agar-based composite hydrogel for multi-mode tumor therapy. *Carbohydr Polym*. 2018;180:112–121.
24. Tomayko MM, Reynolds CP. Determination of subcutaneous tumor size in athymic (nude) mice. *Cancer Chemother Pharmacol*. 1989;24(3):148–154.
25. Yang XY, Li YX, Li M, Zhang L, Feng LX, Zhang N. Hyaluronic acid-coated nanostructured lipid carriers for targeting paclitaxel to cancer. *Caner Lett*. 2013;334(2):338–345.
26. Liu D, Liu F, Liu Z, Wang L, Zhang N. Tumor specific delivery and therapy by double-targeted nanostructured lipid carriers with anti-VEGFR-2 antibody. *Mol Pharm*. 2011;8(6):2291–2301.
27. Needham D, Stoicheva N, Zhelev DV. Exchange of monooleoylphosphatidylcholine as monomer and micelle with membranes containing poly(ethylene glycol)-lipid. *Biophys J*. 1997;73(5):2615–2629.
28. Hu FQ, Jiang SP, Du YZ, Yuan H, Ye YQ, Zeng S. Preparation and characteristics of monostearin nanostructured lipid carriers. *Int J Pharm*. 2006;314(1):83–89.
29. Naguib YW, Rodriguez BL, Li X, Hursting SD, Williams RO III, Cui Z. Solid lipid nanoparticle formulations of docetaxel prepared with high melting point triglycerides: in vitro and in vivo evaluation. *Mol Pharm*. 2014;11(4):1239–1249.
30. Fang G, Tang B, Chao Y, Zhang Y, Xu H, Tang X. Improved oral bioavailability of docetaxel by nanostructured lipid carriers: in vitro characteristics, in vivo evaluation and intestinal transport studies. *RSC Adv*. 2015;5(117):96437–96447.
31. Ernsting MJ, Murakami M, Roy A, Li SD. Factors controlling the pharmacokinetics, biodistribution and intratumoral penetration of nanoparticles. *J Control Release*. 2013;172(3):782–794.
32. Matsumura Y, Maeda H. A new concept for macromolecular therapeutics in cancer chemotherapy: mechanism of tumoritropic accumulation of proteins and the antitumor agent smancs. *Cancer Res*. 1986;46(12 Pt 1):6387–6392.
33. Decuzzi P, Godin B, Tanaka T, et al. Size and shape effects in the biodistribution of intravascularly injected particles. *J Control Release*. 2010;141(3):320–327.
34. Wicki A, Witzigmann D, Balasubramanian V, Huwyler J. Nanomedicine in cancer therapy: challenges, opportunities, and clinical applications. *J Control Release*. 2015;200:138–157.
35. Verma A, Stellacci F. Effect of surface properties on nanoparticle–cell interactions. *Small*. 2010;6(1):12–21.
36. Neves AR, Lúcio M, Martins S, Lima JLC, Reis S. Novel resveratrol nanodelivery systems based on lipid nanoparticles to enhance its oral bioavailability. *Int J Nanomedicine*. 2013;8:177–187.
37. Zhao L, Wei Y, Li W, et al. Solid dispersion and effervescent techniques used to prepare docetaxel liposomes for lung-targeted delivery system: in vitro and in vivo evaluation. *J Drug Target*. 2011;19(3):171–178.
38. Hillaireau H, Couvreur P. Nanocarriers' entry into the cell: relevance to drug delivery. *Cell Mol Life Sci*. 2009;66(17):2873–2896.
39. Teeranachaideekul V, Souto EB, Junyaprasert VB, Müller RH. Cetyl palmitate-based NLC for topical delivery of Coenzyme Q 10 – development, physicochemical characterization and in vitro release studies. *Eur J Pharm Biopharm*. 2007;67(1):141–148.
40. Pawar AA, Chen DR, Venkataraman C. Influence of precursor solvent properties on matrix crystallinity and drug release rates from nanoparticle aerosol lipid matrices. *Int J Pharm*. 2012;430(1):228–237.
41. Son GH, Lee BJ, Cho CW. Mechanisms of drug release from advanced drug formulations such as polymeric-based drug-delivery systems and lipid nanoparticles. *J Pharm Invest*. 2017;47(4):287–296.

42. Kaur P, Garg T, Rath G, Murthy RR, Goyal AK. Development, optimization and evaluation of surfactant-based pulmonary nanolipid carrier system of paclitaxel for the management of drug resistance lung cancer using Box-Behnken design. *Drug Deliv*. 2016;23(6):1912–1925.

43. Souza LG, Silva EJ, Martins AL, et al. Development of topotecan loaded lipid nanoparticles for chemical stabilization and prolonged release. *Eur J Pharm Biopharm*. 2011;79(1):189–196.

44. Selvamuthukumar S, Velmurugan R. Nanostructured lipid carriers: a potential drug carrier for cancer chemotherapy. *Lipids Health Dis*. 2012;11(1):159–166.

45. Zhang X, Gan Y, Gan L, Nie S, Pan W. PEGylated nanostructured lipid carriers loaded with 10-hydroxycamptothecin: an efficient carrier with enhanced anti-tumour effects against lung cancer. *J Pharm Pharmacol*. 2008;60(8):1077–1087.

46. Melikov K, Chernomordik LV. Arginine-rich cell penetrating peptides: from endosomal uptake to nuclear delivery. *Cell Mol Life Sci*. 2005;62(23):2739–2749.

47. Bashyal S, Noh G, Keum T, Choi YW, Lee S. Cell penetrating peptides as an innovative approach for drug delivery; then, present and the future. *J Pharm Invest*. 2016;46(3):205–220.

48. Liu Y, Mei L, Yu Q, et al. Multifunctional tandem peptide modified paclitaxel-loaded liposomes for the treatment of vasculogenic mimicry and cancer stem cells in malignant glioma. *ACS Appl Mater Interfaces*. 2015;7(30):16792–16801.

49. Yamamoto Y, Yoshida M, Sato M, et al. Feasibility of tailored, selective and effective anticancer chemotherapy by direct injection of docetaxel-loaded immunoliposomes into Her2/neu positive gastric tumor xenografts. *Int J Oncol*. 2011;38(1):33–39.

50. Kedmi R, Ben-Arie N, Peer D. The systemic toxicity of positively charged lipid nanoparticles and the role of Toll-like receptor 4 in immune activation. *Biomaterial*. 2010;31(26):6867–6875.

51. Maeda H, Wu J, Sawa T, Matsumura Y, Hori K. Tumor vascular permeability and the EPR effect in macromolecular therapeutics: a review. *J Control Release*. 2000;65(1):271–284.

52. Li X, Xu H, Dai X, Zhu Z, Liu B, Lu X. Enhanced in vitro and in vivo therapeutic efficacy of codrug-loaded nanoparticles against liver cancer. *Int J Nanomedicine*. 2012;7:5183–5190.

53. Bao A, Phillips WT, Goins B, et al. Potential use of drug carried-liposomes for cancer therapy via direct intratumoral injection. *Int J Pharm*. 2006;316(1):162–169.

54. Nomura T, Koreeda N, Yamashita F, Takakura Y, Hashida M. Effect of particle size and charge on the disposition of lipid carriers after intratumoral injection into tissue-isolated tumors. *Pharm Res*. 1998;15(1):128–132.